Available online at www.sciencedirect.com
SCIENCE DIRECT
ELSEVIER
Journal of the European Ceramic Society 26 (2006) 2179–2183
ECERS
www.elsevier.com/locate/jeurceramsoc

FEM simulation of microwave dielectric properties for biphase ceramics

X.C. Fan, X.M. Chen *, L. Li

Department of Materials Science & Engineering, Zhejiang University, Hangzhou 310027, China

Available online 2 November 2005

Abstract

In the present work, microwave dielectric properties of biphase ceramics were calculated via finite element method (FEM) combined with Monte Carlo (MC) simulation. Parameters such as volume fractions, and dielectric constant ratio of two phases were taken into account. Random distribution of tow phases was generated by MC method. Both dielectric constant and *Qf* values were calculated and then numerical fittings were carried out. The simulation results of the dielectric constant were then compared with experiment data and excellent agreement was achieved.

Keyword: Composites; Dielectric properties; FEM

1. Introduction

Since the time of Maxwell, lots of empirical equations have been derived to predict dielectric constant ε_r of composites based on experimental results and theoretical derivation, because in many cases it is very important to precisely predict the dielectric properties.[1,2] For biphase composite, the parallel model, the serial model, the logarithm model and Maxwell–Wagner equation are some of the most well-known ones. However, they cannot give satisfactory results in the full concentration range. Because it is too complicated to obtain analytical solutions in the full concentration range, many researchers have turned towards the help of numeric methods recently.[3–7]

Wakino et al. obtained a new equation for predicting the dielectric constant of a mixture via FEM combined with the MC simulation.[3] The random distribution generated by the MC method is comparatively close to the real situation in a material, and hence a reasonable result can be attained. After the report of a two-dimensional (2D) capacitor model by Wakino et al., Wang et al. reported the result of three-dimensional (3D) model.[4] There was notable difference between results of these two models. The dielectric constant of 3D model was much larger than that of 2D model. It contradicted with the conclusion by Wakino et al.: when 2D model was extended to the 3D case, there would not be significant changes in results.[3] More work should be done to justify which is correct. Besides, they did not calculate the loss tangent of a mixture and did not take into account of the effect of dielectric constant ratio of two phases. In recent years, Brosseau et al. have published a series of articles on the modeling of both dielectric constant and loss tangent by FEM and the boundary integral equation method.[6] But their studies were mainly concerned on biphase periodic composite and the effective dielectric constant of their 3D random composites model was computed by considering the equivalent periodic material.[7]

In the family of microwave dielectric ceramics, biphase ceramics play an important role,[8–10] so in the present work, capacitor models were built for biphase microwave dielectric ceramics. The random distribution of biphase composite was generated by MC method. Both dielectric constant and loss tangent were calculated via FEM and the results were fitting to obtain new equations. The modeling results were then compared with experiments data.

2. Calculation method

In this paper, volume fraction, relative dielectric constant and electric filling factor are denoted as V, ε_r and P_e, respectively. Besides, subscripts "1", "2" or none are added to distinguish variables of material 1, material 2 and composite.

The FEM calculation procedures are introduced in many literatures[4,11] and books,[12] so we would not mention it here, except for three points:

(1) In our simulation, 20-node hexahedral elements were used.
(2) The random distribution was generated via MC method which had been mentioned by Wakino et al.[3] But our model

* Corresponding author. Tel.: +86 571 8795 2112; fax: +86 571 8795 2112.
E-mail address: xmchen@cmsce.zju.edu.cn (X.M. Chen).

0955-2219/$ – see front matter © 2005 Elsevier Ltd. All rights reserved.
doi:10.1016/j.jeurceramsoc.2005.09.076

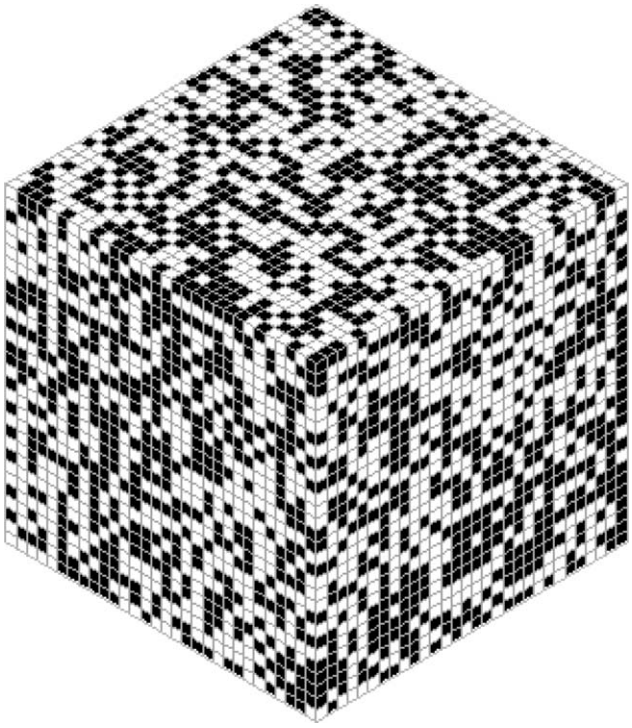

Fig. 1. The cubic is divided into $30 \times 30 \times 30$ subcubic cells. One possible random distribution generated by Monte Carlo method for $V_1{:}V_2 = 0.5{:}0.5$ is shown.

is cubic and it was divided into $30 \times 30 \times 30$ subcubic cells. One possible random distribution is plotted in Fig. 1 for $V_1{:}V_2 = 0.5{:}0.5$.

(3) Electric filling factor and *Qf* value are calculated using:

$$P_{ei} = \frac{(1/2)\iiint_{V_i} \varepsilon_{ri} \vec{E}\vec{E}^* \, dV}{(1/2)\iiint_{V} \varepsilon_r(V) \vec{E}\vec{E}^* \, dV} \quad (1)$$

and

$$Qf = \left(\frac{1 - P_{e2}}{Qf_1} + \frac{P_{e2}}{Qf_2} \right)^{-1} \quad (2)$$

where the numerator on the right hand of Eq. (1) is the electric energy stored in all elements of *i*th material, and the denominator is the total electric energy stored in the whole capacitor.

In the simulation, ε_{r1} was kept to be 1, and ε_{r2} was chosen to be 3, 10, 20 and 100. V_2 was chosen to be 0, 0.01, . . ., 0.06, 0.08, 0.1, 0.2, . . ., 0.9, 0.94, 0.98 and 1. The simulation process was repeated at least 20 times on each compound. Then the mean value, as well as standard deviation was calculated.

3. Results and discussion

In Table 1, average values $\langle \varepsilon_r \rangle$, $\langle P_{e2} \rangle$and their standard deviations (S.D.) with respect to the number of divisions (Ndiv) are shown for $\varepsilon_{r2} = 100$ and $V_2 = 0.5$. With increase of Ndiv, $\langle \varepsilon_r \rangle$, $\langle P_{e2} \rangle$ and their S.Ds. gradually converge; when Ndiv > 30, all these parameters change little. To balance consuming time and precision of calculation, $30 \times 30 \times 30$ divisions were considered to be accurate enough for the simulation.The following equation

Table 1
Average value $\langle \varepsilon_r \rangle$, $\langle P_{e2} \rangle$ and their standard deviations (S.D.) with a changing number of divisions (Ndiv) when $\varepsilon_{r2} = 100$ and $V_2 = 0.5$

Ndiv	$\langle \varepsilon_r \rangle$	S.D.	$\langle P_{e2} \rangle$	S.D.
5	32.06	2.36	0.958	0.0089
10	32.59	0.96	0.959	0.0034
15	32.74	0.41	0.960	0.0015
20	33.00	0.32	0.961	0.0010
25	33.05	0.24	0.961	0.0008
30	33.18	0.13	0.961	0.0004
35	33.21	0.12	0.962	0.0004

was obtained by Wakino et al.[3]:

$$\varepsilon_r^\alpha = V_1 \varepsilon_{r1}^\alpha + V_2 \varepsilon_{r2}^\alpha, \quad \alpha = V_2 - V_0 \quad (3)$$

where V_0 is the critical volume fraction and equals to round about 0.35 given $\varepsilon_{r1} < \varepsilon_{r2}$. In Eq. (3), α is linear with respect to V_2. Because the form of Eq. (3) is a general one of many mixing rules, it would be used to fit our simulated results with a different expression of α. After $\langle \varepsilon_r \rangle$ of each compound was obtained, index α was calculated and plotted as scatters in Fig. 2. As shown in Fig. 2, index α is a function of mixing ratio and dielectric constant ratio of two phases. For all ratios of ε_{r2} to ε_{r1}, index α increases when V_2 grows. When $\varepsilon_{r2} = 3$, the relation between α and V_2 is quasi-linear, but when ε_{r2} increases, it becomes more and more non-linear. Besides, when V_2 is small, α decrease with the dielectric constant ratio enlarges while when V_2 is large, the opposite situation occurs. After several trials, it was found that the function shown in Eq. (4) fitted the calculated α best in a least-squares sense. The coefficients are listed in Table 2.

$$\varepsilon_r^\alpha = V_1 \varepsilon_{r1}^\alpha + V_2 \varepsilon_{r2}^\alpha, \quad \alpha = A_2 + \frac{A_1 - A_2}{(1 + (V_2/u_0)^p)} \quad (4)$$

Curves of α calculated by Eq. (4) are plotted as solid lines in Fig. 2 for $\varepsilon_{r2} = 3$, 10, 20 and 100. Good agreement is achieved between simulation results and Eq. (4)

In Fig. 3, curves of $\langle \varepsilon_r \rangle$ calculated in our present work and the dielectric constants calculated by the parallel model, the serial

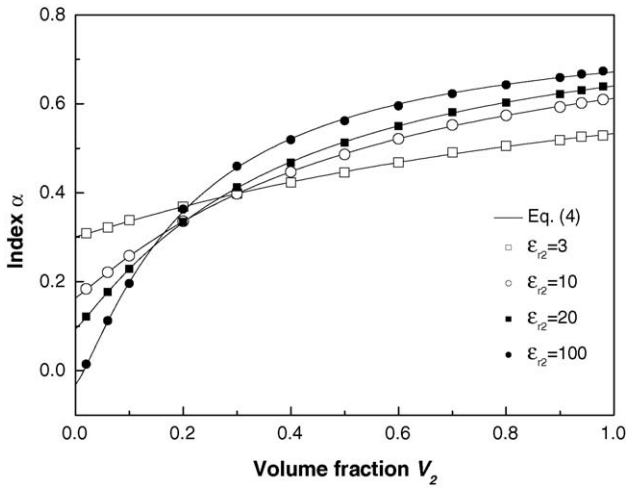

Fig. 2. Index α of Eq. (4) with respect to volume fraction V_2 and relative dielectric constant ε_{r2} of material 2.

Table 2
Coefficients of α in Eq. (4) and P_{e2} in Eq. (5) for $\varepsilon_{r2}:\varepsilon_{r1} = 3$, 10, 20 and 100

$\varepsilon_{r2}:\varepsilon_{r1}$	A_1	A_2	u_0	p	B_2	w_0	q
3	0.301	0.812	1.186	1.055	1.914	0.927	1.190
10	0.164	0.849	0.552	1.078	1.165	0.338	1.660
20	0.093	0.832	0.387	1.106	1.068	0.254	1.958
100	−0.032	0.780	0.214	1.215	1.007	0.166	2.751

model, the logarithmic mixing rule, the Maxwell–Wagner equation and Eq. (3) are plotted for $\varepsilon_{r2} = 100$. The bold solid line is plotted according to Eq. (4) and coefficients for $\varepsilon_{r2}:\varepsilon_{r1} = 100$ in Table 2. It is in good agreement with simulated results, which are plotted as open circles.

As shown in Fig. 3, the curve obtained in our present work is closer to the curve of the parallel model than the one calculated by Eq. (3). Just as mentioned before, a quite similar result had been reported by Wang et al. Our model and Wang's model were both 3D, while Wakino's one was 2D. For 2D model, the dimensions parallel and perpendicular to electric flux are both 1, while for 3D one, dimension perpendicular to electric flux retains 1, but the dimension parallel to electric flux increases to 2. We can consider an extreme simple example: when $V_1:V_2 = 0.5:0.5$, for a 2D model with 2×2 grid size, the probabilities of parallel case and serial case are both 1/3 and their ratio is 1:1; while for a 3D model with $2 \times 2 \times 2$ grid size, the probabilities of parallel case and serial case are 3/35 and 1/35 and their ratio becomes 3:1. So according to the statistical distribution theory, the most possible distribution of 3D MC model is closer to the parallel model, compared with 2D MC model; this conclusion can extend to models with larger grid size.

The electric filling factor P_{e2} is also calculated for $\varepsilon_{r2}:\varepsilon_{r1} = 3$, 10, 20 and 100, and plotted as scatters in Fig. 4. As Fig. 4 (a) shown, with increase of V_2, P_{e2} grows from zero to one; when V_2 retains the same and ε_{r2} enlarges, P_{e2} increases; when $\varepsilon_{r2} = 3$, the change of P_{e2} versus V_2 is quasi-linear, but when ε_{r2} increases, the shape of curve becomes more and more like a hill. If we compare Fig. 2 and Fig. 4(a), we will find that there are many similarities between them, and this is because the index α and

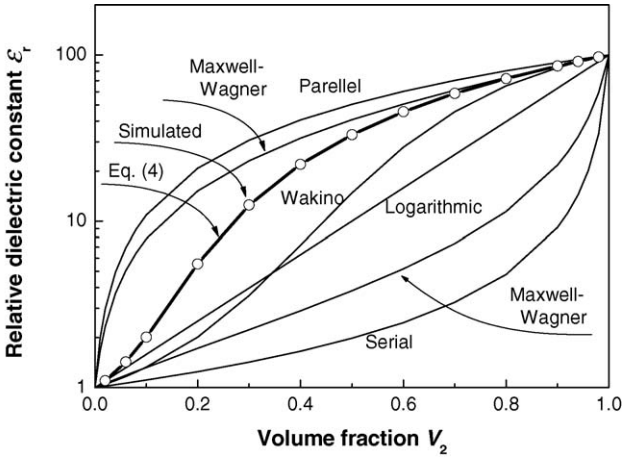

Fig. 3. Comparison of several predictive equations of dielectric constant given $\varepsilon_{r1} = 1$ and $\varepsilon_{r2} = 100$.

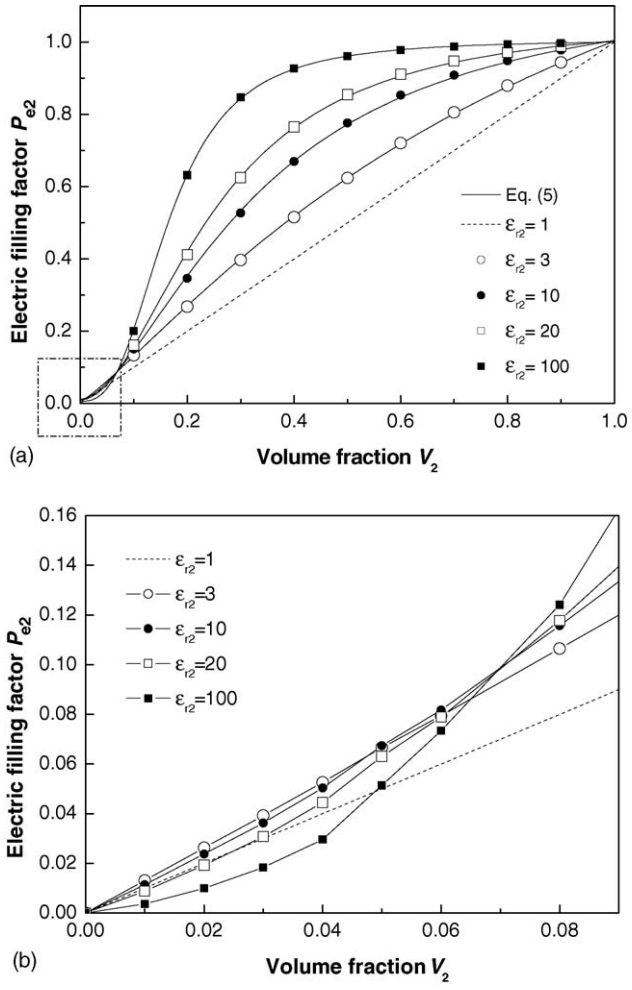

Fig. 4. (a) Electric filling factor P_{e2} calculated by FEM and Eq. (5) in the full concentration range. (b) Magnification of the part which is enclosed in a dash dot rectangular in (a).

P_{e2} both reflect the energy distribution in two phases. So the function used to fit α was found to fit P_{e2} best too and rewritten as Eq. (5). The coefficients of Eq. (5) for $\varepsilon_{r2}:\varepsilon_{r1} = 3$, 10, 20 and 100 are listed in Table 2.

$$P_{e2} = B_2 - \frac{B_2}{1 + (V_2/w_0)^q} \tag{5}$$

The solid lines in Fig. 4(a) are plotted by Eq. (5) and corresponding coefficients. It is very interesting to note that these curves intercept each other when V_2 is small, just as the region enclosed in a dash dot rectangular shown. This region is magnified and more points of V_2 are added in Fig. 4(b). We can note that with increase of ε_{r2}, P_{e2} first increases and then drops given V_2 keeps the same and is sufficiently small. This can be explained by Eq. (1). When V_2 is small, the total energy, i.e. the dinominator of Eq. (1) change little with increase of ε_{r2}, but the energy stored in material 2 first increase because of the increase of ε_{r2} and then drops because of quick decay of the square of electric field strength magnitude.

For $\varepsilon_{r2} = 3$ and 100: when $V_2 \leq 0.07$, P_{e2} of the latter is smaller than that of the former. It means than the Qf value of the latter is larger than that of the former when $V_2 \leq 0.07$, given

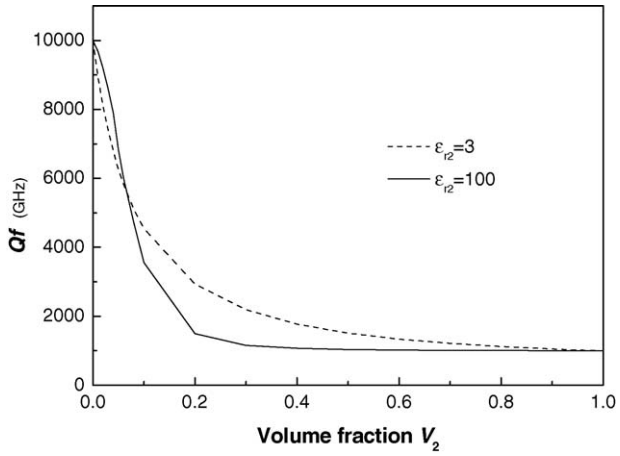

Fig. 5. Qf value for $\varepsilon_{r2} = 3$ and 100, given $Qf_1 = 10000$ GHz and $Qf_2 = 1000$ GHz.

$Qf_1 = 10{,}000$ GHz and $Qf_2 = 1000$ GHz, just as shown in Fig. 5. We expect Qf value calculated by Eq. (2) will be close to the actual value when one phase is sufficiently dilute and the boundary effect of two phases is not prominent.

4. Experiment verification

To evaluate the performance of Eq. (4) with actual data, we performed the following experiment. $(1-x)MgTiO_3$–$xCaTiO_3$ ceramics with $x = 0, 0.05, 0.25, 1/3, 0.5, 2/3, 0.75$ and 1 were prepared by a routine solid state reaction process where the reagent grade MgO (97%), CaO (99.0%) and TiO_2 (99.5%) powders were used as the raw material. All samples were sintered at 1375 °C in air for 3 h. Diameter and height of each sample were around 10.6 mm and 5 mm. Density ρ was measured by Archimedes method and ε_r was measured at 2–10 GHz by Hakki and Coleman method.[13,14] Measured ρ for $MgTiO_3$ and $CaTiO_3$ were 3.67 g/cm^3 and 3.94 g/cm^3, measured ε_r for $MgTiO_3$ and $CaTiO_3$ were 17.2 and 178.9. Then the volume fractions of $CaTiO_3$ were calculated by mole fractions of $CaTiO_3$, molecular weights and measured densities of $MgTiO_3$ and $CaTiO_3$. Then Eq. (4) with coefficients listed in Table 2 for ε_{r2}:$\varepsilon_{r1} = 10$, the parallel model, the serial model, the logarithmic mixing rule and Eq. (3) obtained by Wakino et al. were used to calculate the dielectric constant of $(1-x)MgTiO_3$–$xCaTiO_3$. All the results are listed in Table 3. XRD showed that $MgTi_2O_5$ phase existed when $x < 1$; it is very common that $MgTi_2O_5$ coexists with $MgTiO_3$[15–17] and it will not affect the validity of our results.

Table 3
Comparison between measured data and results calculated by several predictive equations for $(1-x)MgTiO_3$–$xCaTiO_3$ ceramics

x	ρ (g/cm^3)	V_2	ε_r					
			Meas.	Eq. (4)	Para.	Serial	Log.	Wakino
0	3.67	0	17.2	17.2	17.2	17.2	17.2	17.2
0.05	3.68	0.053	20.1	20.1	25.7	18.1	19.5	18.8
0.25	3.74	0.260	37.7	39.5	59.2	22.5	31.6	30.2
1/3	3.76	0.345	49.1	51.0	73.0	25.0	38.6	38.5
0.5	3.82	0.513	77.7	78.6	100.2	32.1	57.2	63.9
2/3	3.84	0.678	110.0	110.2	126.9	44.5	84.2	100.5
0.75	3.86	0.760	127.7	126.9	140.1	54.9	101.9	120.9
1	3.94	1	178.9	178.9	178.9	178.9	178.9	178.9

As shown in Table 3, an excellent agreement between Eq. (4) and measured data was achieved. Some more work needs to be done to evaluate Eq. (2) combined with Eq. (5) for a dilute inclusion situation; it will be done in our future work.

5. Conclusion

Three-dimensional capacitor models were built and the effective dielectric constant and loss tangent of biphase composite were calculated via FEM combined with Monte Carlo simulation. From above discussion, we can conclude that:

(1) Simulation results show that 3D MC model is closer to the parallel model than 2D MC model; this may be explained by statistical distribution theory.
(2) The effective dielectric constant of biphase composite is a non-linear function of dielectric constant ratio and volume fractions of two phases. A new equation was obtained for 3D MC model:

$$\varepsilon_r^{\alpha} = V_1\varepsilon_{r1}^{\alpha} + V_2\varepsilon_{r2}^{\alpha}, \quad \alpha = A_2 + \frac{A_1 - A_2}{1 + (V_2/u_0)^p}$$

where the coefficients are listed in Table 2. Experiments of $MgTiO_3$-$CaTiO_3$ verified its validity.
(3) The electric filling factor for 3D MC model can be fitted as following:

$$P_{e2} = B_2 - \frac{B_2}{1 + (V_2/w_0)^q}$$

where the coefficients are listed in Table 2.

Acknowledgement

The present work was partially supported by Chinese National Key Project for Fundamental Researches under grant No. 2002CB613302, National Science Foundation of China under grant No. 50332030 and National Science Foundation for Distinguished Young Scholars under grant No. 50025205.

References

1. Tinga, W. R., Voss, W. A. G. and Bossey, D. F., Generalized approach to multiphase dielectric mixture theory. *J. Appl. Phys.*, 1973, **44**, 3897–3902.
2. Milton, G. W., Bounds on the complex permittivity of a two-component composite material. *J. Appl. Phys.*, 1981, **52**, 5286–5293.
3. Wakino, K., Okada, T., Yoshida, N. and Tomono, K., A new equation for predicting the dielectric constant of a mixture. *J. Am. Ceram. Soc.*, 1993, **76**, 2588–2594.
4. Wang, G. Q., Wu, S. H., Zhao, Y. S. and Zhang, Z. P., 3-Dimensionalal simulation of the interior electric field and macro dielectric constant of a tow-phase composite material. *J. Inorg. Mater.*, 2004, **19**, 214–222 (in Chinese).
5. Chen, A., Yu, Z., Guo, R. and Bhalla, A. S., Calculation of dielectric constant and loss of two-phase composites. *J. Appl. Phys.*, 2003, **93**, 3475–3480.

6. Sareni, B., Krähenbühl, L. and Beroual, A., Effective dielectric constant of random composite materials. *J. Appl. Phys.*, 1997, **81**, 2375–2383.
7. Brosseau, C. and Beroual, A., Computational electromagnetics and the rational design of new dielectric heterostructures. *Prog. Mater. Sci.*, 2003, **48**, 373–456.
8. Wakino, K., Recent development of dielectric resonator materials and filters in Japan. *Ferroelectrics*, 1989, **91**, 69–86.
9. Katoh, T. and Ozeki, H. Microwave dielectric ceramic composition. US Patent 5,340,784, 23 August 1994.
10. Liu, X. Q. and Chen, X. M., Microstructures and dielectric properties of $CaTiO_3$–$LaSrAlO_4$ composite ceramics. *Mater. Sci. Eng.*, 2004, **B110**, 296–301.
11. Kooi, P. S. *et al.*, Finite-element analysis of the shielded cylindrical dielectric resonator. *IEE Proc.*, 1985, **132**, 7–16.
12. Zeng, Y. G., Xu, G. H. and Song, G. X., *Electromagnetic field finite element method*. Science Press, Beijing, 1982 (in Chinese).
13. Hakki, B. W. and Coleman, P. D., A dielectric resonator method of measuring inductive capacities in the millimeter range. *IRE Trans. Microwave Theory Tech.*, 1960, **8**, 402–410.
14. Courtney, W. E., Analysis and evaluation of a method of measuring the complex permittivity and permeability of microwave insulators. *IEEE Trans. Microwave Theory Tech.*, 1970, **18**, 476–485.
15. Ferreira, V. M., Baptista, J. L., Kamba, S. *et al.*, Dielectric spectroscopy of $MgTiO_3$-based ceramics in the 10^9–10^{14} Hz region. *J. Mater. Sci.*, 1993, **28**, 5894–5900.
16. Sato, T., Miyamoto, R. and Fukasawa, A., Deviation of dielectric properties in magnesium titanate ceramics. *Jpn. J. Appl. Phys.*, 1981, **20**, 151–154.
17. Wang, K. S., Luo, L., Chen, W. and Zhang, G. C., Effects of Al_2O_3 on the microwave dielectric properties of $MgTiO_3$ ceramics. *J. Inorg. Mater.*, 2002, **17**, 509–514 (in Chinese).